NACA TN 2285

NATIONAL ADVISORY COMMITTEE FOR AERONAUTICS

TECHNICAL NOTE 2285

DAMPING IN ROLL OF CRUCIFORM AND SOME RELATED DELTA WINGS AT SUPERSONIC SPEEDS

By Herbert S. Ribner

Lewis Flight Propulsion Laboratory
Cleveland, Ohio

Washington
February 1951

ERRATA

NACA TN 2285

DAMPING IN ROLL OF CRUCIFORM AND SOME RELATED
DELTA WINGS AT SUPERSONIC SPEEDS
By Herbert S. Ribner

February 1951

Page 5: Equation (9) should read

$$C_{l_p} = -\frac{2m}{\beta\pi}$$

Page 23: The definition of C_{l_p} should read

$$\text{damping-in-roll derivative} = \frac{\text{rolling moment}}{\frac{1}{2}\rho V^2 \cdot \text{area two panels} \cdot 2s \cdot \frac{ps}{V}}$$

Page 43, figure 13: The curve labeled "Equation (32)" should be labeled "Equation (30)."

NACA-Langley - 4-17-52 - 1025

NATIONAL ADVISORY COMMITTEE FOR AERONAUTICS

TECHNICAL NOTE 2285

DAMPING IN ROLL OF CRUCIFORM AND SOME RELATED DELTA WINGS AT SUPERSONIC SPEEDS

By Herbert S. Ribner

SUMMARY

The damping in roll of cruciform delta wings in supersonic flow has been evaluated by means of small-disturbance (linearized) wing theory; both subsonic and supersonic component stream velocities normal to the leading edges have been considered. In addition, some known two-dimensional results for rotating multibladed laminae have been applied to obtain the loading when the number of panels is changed from four to an arbitrary number, under the restriction of low aspect ratio; the damping in roll has been determined explicitly for three panels. Finally, the damping for an infinite number of panels has been evaluated without restriction as to aspect ratio or Mach number.

INTRODUCTION

The linearized theory of planar wings in supersonic flow has been highly developed. The theory for nonplanar wings such as the cruciform seems to have been limited, until very recently, to the analysis (reference 1) of the cruciform delta wing with angle of attack and sideslip. The rolling behavior of a cruciform delta wing is likewise of considerable importance in flight mechanics. The present paper is concerned primarily with the evaluation of the damping in roll.

The cruciform delta wing is illustrated in figure 1(a). This type of wing develops a large side force when sideslipped, thus permitting sharp turns without banking. With or without sideslip, the problem of calculating the lift distribution is simple because the horizontal and vertical wings behave as though they were isolated.

For rolling motion, however, the situation is more complex. The horizontal and vertical wings mutually interfere, so that the pressure distributions are not the same as if the wings were isolated. The calculation is no longer a planar problem, and the well-known planar techniques in linearized wing theory must be extended.

For the very narrow (low-aspect-ratio) cruciform, the Munk-Jones approximate theory (reference 2) may be applied. The problem reduces to the determination of the potential of a rotating cruciform lamina in two-dimensional flow. This problem has already been solved in connection with propeller theory; in addition, the problem of the rotating lamina has been solved (in series form) for any finite number of blades (reference 3). This work is discussed and applied in the section "Low-Aspect-Ratio Approximation for Multiplanar Wings."

The case of a broad cruciform wing with supersonic leading edges may readily be reduced to a planar boundary-value problem. The principles of superposition and reflection are used. When the leading edges are subsonic, a partial reduction to a planar problem is still possible. The solution is then completed by an iteration procedure of rapid convergence. The simpler supersonic-edge case is treated in the section "Cruciform with Supersonic Leading Edges" and the subsonic-edge case is treated in the section "Cruciform with Subsonic Leading Edges."

Two contemporary investigations covering portions of the scope of the present investigation have recently been noted. The slender cruciform has been treated by Gaynor J. Adams of the NACA Ames laboratory. The cruciform delta with supersonic leading edges is reported in reference 4. The cruciform delta with subsonic leading edges, which occupies most of the present investigation, apparently has not been treated elsewhere.

LOW-ASPECT-RATIO APPROXIMATION FOR MULTIPLANAR WINGS

Arbitrary Number of Panels

The multiplanar wing under consideration is illustrated in figure 1(b). Each panel is an identical right triangle, and the long leg is common; the cross section perpendicular to this leg presents a spoke-like appearance. The damping in roll about the axis of symmetry is to be calculated.

The restriction to low aspect ratio (triangular panels very slender) allows the approximate theory of reference 1 to be employed; the results apply for subsonic, transonic, and a range of supersonic speeds. According to this theory the local potential at any section perpendicular to the axis of symmetry is approximately the same as if the section were a two-dimensional lamina. The present problem is thus reduced to the determination of the potential distribution on a two-dimensional lamina of N equally spaced spokes, rotating about the center.

It happens that a similar reduction of the problem of the wake of a multiblade propeller is possible. As the wake pitch approaches infinity, that problem likewise reduces to that of the two-dimensional rotating lamina. In this connection, the potential distribution for the lamina was obtained in reference 3; there is evaluated therein a function K that is related to the surface-potential jump $\Delta\phi$ by

$$\Delta\phi = \frac{2\pi r^2 p}{N} K$$

in the present notation. This equation, together with the equation for K in reference 3 (p. 682), gives the series for the potential jump

$$\Delta\phi = 2^{2-4/N} s^2 p \frac{\Gamma(1+4/N)}{\left[\Gamma(1+2/N)\right]^2} \sum_{n=1}^{\infty} (-1)^{n+1} \frac{(N-2)(2N-2)\ldots(nN-N-2)}{(N+2)(2N+2)\ldots(nN+2)} \sin Nn\theta \tag{1}$$

where the parameter θ is defined by

$$r = s\left(\cos\frac{1}{2}N\theta\right)^{2/N}$$

and r is the radial distance. The series "is troublesome to handle analytically but is quite convenient for numerical computation."

Three Panels

The insertion of $N = 3$ reduces equation (1) to

$$\Delta\phi = 2^{2/3} s^2 p \frac{\Gamma(1/3)}{\left[\Gamma(2/3)\right]^2} \sum_{n=1}^{\infty} (-1)^{n+1} \frac{1\cdot 4\cdot\cdot\cdot(3n-5)}{5\cdot 8\cdot 11\cdot\cdot\cdot(3n+2)} \sin 3n\theta \tag{2}$$

with $r = s\left[\cos(3\theta/2)\right]^{2/3}$

The series in equation (2) has been summed numerically in reference 3. The results have been used to obtain the values of $\frac{N\Delta\phi}{s^2 p}$ against r/s tabulated in table I.

The rolling moment developed by the three panels is given by

$$L = -3\rho V \int_0^s \Delta\phi \, r \, dr$$

The integration has been performed graphically and the result is

$$L = -0.531 \, \rho V p s^4 \tag{3}$$

with about 1 percent uncertainty.

This damping compares with that (reference 5) for the flat, narrow delta (2 panels) as follows

$$\frac{\text{damping in roll, } N = 3}{\text{damping in roll, } N = 2} = 1.35 \pm 0.014 \tag{4}$$

This ratio is about 10 percent less than the ratio 1.5 that would be obtained from an elementary calculation neglecting interference. The reduction is caused by mutual interference among the three panels.

Four Panels (Cruciform)

The insertion of $N = 4$ reduces equation (1) to

$$\Delta\phi = \frac{4}{\pi} s^2 p \sum_{n=1}^{\infty} (-1)^{n+1} \frac{\sin 4n\theta}{4n^2-1} \tag{5}$$

This series may be summed, and according to reference 3 the result is

$$\Delta\phi = \frac{2}{\pi} s^2 p \cos 2\theta \log_e \frac{1+\tan\theta}{1-\tan\theta} \tag{6}$$

with $r = s\sqrt{\cos 2\theta}$. The span loading is proportional to $\Delta\phi$; the variation of $\frac{N\Delta\phi}{s^2 p}$ with r/s is given in table I.

The rolling moment developed by the four panels is given by

$$L = -4\rho V \int_0^s \Delta\phi \, r \, dr = -\frac{2\rho V p s^4}{\pi} \tag{7}$$

Comparison with the flat, narrow delta (two panels) gives

$$\frac{\text{damping in roll, } N = 4}{\text{damping in roll, } N = 2} = \frac{16}{\pi^2} = 1.62 \tag{8}$$

If there were no mutual interference between the panels, the factor would be 2. The loss in damping caused by the interference is thus 19 percent for the narrow cruciform delta.

The nondimensional damping-in-roll derivative C_{l_p} for the narrow cruciform is obtained by dividing equation (7) by $\rho V p s^4 \beta / m$. The resulting coefficient, which is based on the area of just two of the four panels, is

$$C_{l_p} = -\frac{2m}{\pi} \tag{9}$$

Infinite Number of Panels

Equation (1) is inconvenient for evaluating the behavior when the configuration has an infinite number of panels ($N = \infty$). The result can be obtained, however, from simple physical considerations, which need not be limited to the case of a narrow wing. Fix attention on the section perpendicular to the axis in figure 2, and imagine the number of panels greatly increased. Qualitatively, the air trapped between the panels will tend to move as a unit with the blades; so will the cylindrical wake. (The centrifugal forces acting on the rotating air mass are second-order effects proportional to p^2 and hence may be neglected in the present analysis.) Furthermore, the external disturbance will be like that near the edges of a moving cascade: this disturbance will be appreciable only

within radial distances comparable with the gap distance between panels at the periphery. In the limit, then, as the number of panels becomes infinite, the external disturbance vanishes, and the interior fluid (that within the conical envelope of the panels together with the cylindrical wake) rotates as a solid.

This result may be proved as follows: Assume that $\Delta\phi$, which is equal to the circulation Γ, varies as r^2 in the radial direction along the panel and is independent of x. This implies that the loading is concentrated along the leading edge and that $d\Gamma/dr$ varies as r. The total circulation threading an annulus of radial thickness dr, coaxial with the multiplanar wing, is $\frac{Nd\Gamma}{dr}\,dr$. The mean vorticity in this annulus is the circulation divided by the area $2\pi r\,dr$. This vorticity is $\frac{Nd\Gamma/dr}{2\pi r}$, which is independent of r. As the number of panels N approaches infinity the vorticity approaches a uniform distribution within the annulus. Because there is no change from one annulus to another (independence of r), the vorticity is uniform over the entire circular cross section normal to the axis. This property holds for all such cross sections from the apex of the multiplanar wing back into the cylindrical wake.

Such a uniform distribution of vorticity implies that the fluid bounded by the conical envelope of the wing and the cylindrical surface of the wake rotates as solid. The outer fluid is completely undisturbed, because a surface sheath of vorticity of reversed sign achieves exact cancellation of the disturbance farther out. This surface sheath results from the discontinuous drop of Γ to zero at the edge of each panel $\left(\frac{d\Gamma}{dr} = -\infty\right)$. The rotation of the interior fluid as a solid clearly complies with the boundary conditions at the panels. Moreover, the Prandtl-Glauert partial differential equation is satisfied between the panels and in the outer space. Thus the assumed parabolic distribution of $\Delta\phi = \Gamma$ (which may be interpreted as a distribution either of doublets or vortices) satisfies the boundary-value problem and must be the correct solution.

The damping in roll may now be evaluated either by considerations of angular momentum or of individual panel loading. The momentum approach is given because of its greater simplicity; the panel-loading approach gives identical results. The torque or rolling moment is equal to the time rate of increase of the angular momentum of the wake. This may be written

$$L = -IpV$$

where I is the moment of inertia per unit length of the cylindrical rigidly rotating wake. Insertion of the value $\frac{\pi}{2}\rho s^4$ for I yields

$$L = -\frac{\pi}{2}\rho V p s^4 \tag{10}$$

Comparison of this damping moment with that for a flat, narrow delta ($N = 2$) gives the proportion

$$\frac{\text{damping in roll, } N = \infty}{\text{damping in roll, } N = 2} = \frac{4}{1} \tag{11}$$

In other words, the addition of an infinite number of similar panels radially disposed to a flat narrow delta wing increases the total damping in roll by just a factor of 4.

The foregoing analysis for an infinite number of panels does not involve the assumption that the panels are slender nor any restriction on the Mach number. Thus the damping-in-roll equation (10), unlike the corresponding equations for three and four panels, is valid for all aspect ratios and any speed, subsonic or supersonic, so long as the disturbances are small.

CRUCIFORM WITH SUPERSONIC LEADING EDGES

Assumptions. - The assumptions of an inviscid fluid and small disturbances (isentropic flow) have been made throughout this paper. Thus the disturbance velocities u,v,w possess a potential ϕ that satisfies the linearized equation of motion

$$(1-M^2)\phi_{xx} + \phi_{yy} + \phi_{zz} = 0 \tag{12}$$

known as the Prandtl-Glauert equation. To the first order, the relation between pressure and velocity disturbances is

$$P = -\rho V u \tag{13}$$

where

$$u \equiv \phi_x$$

Analysis. - The boundary conditions for the cruciform wing rolling clockwise with angular velocity p are shown in figure 2. The conditions are

$$w = - py$$

on the horizontal panels, and

$$v = pz$$

on the vertical panels; in addition, u, v, and w must vanish outside the envelope of the Mach cones from the apex and the leading edges.

The flow in each quadrant is the same, except for orientation, because of the fourfold symmetry. It will thus suffice to limit attention to the first quadrant, defined by AOB. Because of the linearity of equation (12), the principle of superposition may be used. Accordingly, the flow specified by the boundary conditions on AOB (redrawn in fig. 3) may be obtained by the linear superposition of the flows defined as 3(b) and 3(c).

The general character of the flow specified by the boundary conditions labeled Flow 3(b) may be anticipated. The value of u will differ from zero on both OA and OB. Call the value on OA (upper surface) u_A, and the value on OB (right-hand surface) u_B. Now flow 3(c) is just a mirror image of flow 3(b) rotated through 90° with sign change. This flow is characterized by a u-velocity $-u_A$ along OB and a u-velocity $-u_B$ along OA. Superposition yields the resultant values:

$$\Sigma u = (\Sigma u)_A = u_A - u_B \tag{14}$$

along the upper surface of OA, and

$$\Sigma u = (\Sigma u)_B = - (u_A - u_B) \tag{15}$$

along the right-hand surface of OB.

The problem of calculating the pressure distribution on the rolling cruciform wing (fig. 2) has now been reduced (equation (13)) to the problem of calculating u_A and u_B for flow 3(b). This problem is easily solved by the method of images. The method is applicable because the vertical panel OB completely isolates disturbances from the left and right sides. Thus consider figure 4(b). The right-hand side is identical with the figure specifying flow 3(b), and the left-hand side is a mirror image, the

combination being symmetrical about OB. The symmetry automatically satisfies the condition $v = 0$ along OB. By virtue of the symmetric linear variation of angle of attack, the delta wing COA is called a wing of linear twist or linear washin.

Solution for u_A. - The calculation will employ figure 4(a). Regions I and II, separated by the Mach cone from the apex, must be distinguished. Region I is uninfluenced by the remainder of the wing, and the pressure distribution and u-velocity there are the same as for an isolated rolling delta wing. The value for u therein may be taken from reference 6, table II, or reference 7. In the present notation it is

$$u_{A,I} = \frac{pm^2x\,(m\sigma-1)}{\beta^2\,(m^2-1)^{3/2}} \qquad \text{region I} \tag{16}$$

where $\sigma = \beta y/x$

The solution for the u-velocity in region II may be effected by standard methods (for example, reference 8). The result is

$$u_{A,II} = \frac{-pm^2x}{\pi\beta^2(m^2-1)^{3/2}}\left[-2\sqrt{(m^2-1)(1-\sigma^2)} + (1-m\sigma)\cos^{-1}\frac{1-m\sigma}{m-\sigma} + (1+m\sigma)\cos^{-1}\frac{1+m\sigma}{m+\sigma}\right] \tag{17}$$

Solution for u_B. - Equation 3 of reference 8 gives the surface u-velocity in terms of a surface integral of $\partial w/\partial x$ and a line integral of the value of w along the leading edge. The formula is easily generalized to values of u above the surface. For the present case, only the line integral survives and

$$u_B = u_B(x,0,z)$$

$$= -\frac{1}{\pi}\int_{L.E.}\frac{w\,dy_1}{\sqrt{(x-x_1)^2-\beta^2y_1^2-\beta^2z^2}}$$

On the wing $w = -p\,|y_1|$ and along the leading edge $\beta\,|y_1| = mx_1$. Because of the symmetry, the integral can be doubled and limited to the right-hand leading edge. The substitutions yield

$$u_B = \frac{2pm^2}{\pi\beta^2} \int_0^{M.C.} \frac{x_1\,dx_1}{\sqrt{(x-x_1)^2 - m^2x_1^2 - \beta^2z^2}}$$

where M.C. denotes the value of x_1 on the Mach cone, where the square root vanishes. Finally

$$u_B = \frac{2pm^2x}{\pi\beta^2(m^2-1)^{3/2}} \left[\sqrt{(m^2-1)(1-\sigma^2)} - \tan^{-1}\sqrt{(m^2-1)(1-\sigma^2)}\right] \quad (18)$$

where σ has been written for $\beta z/x$. If, now, the earlier significance $\beta y/x$ is restored to σ, equation (18) may be applied along OA (fig. 3(a)) as desired. When the leading edges are sonic, $m = 1$, and by application of a limiting process, equation (18) is seen to reduce to

$$u_B = \frac{2px}{3\pi\beta^2}(1-\sigma^2)^{3/2} \quad (19)$$

Resultant u-velocity and pressure distribution. - In region I u_B vanishes; therefore, according to equations (14) and (16),

$$(\Sigma u)_I = u_{A,I}$$

$$= \frac{pm^2x\,(m\sigma-1)^{3/2}}{\beta^2(m^2-1)} \qquad \text{region I} \quad (20)$$

For region II, substitution of equations (17) and (18) in equation (14) gives

$$(\Sigma u)_{II} = \frac{-pm^2x}{\pi\beta^2(m^2-1)^{3/2}}\left[-2\tan^{-1}\sqrt{(m^2-1)(1-\sigma^2)} + (1-m\sigma)\cos^{-1}\frac{1-m\sigma}{m-\sigma} + (1+m\sigma)\cos^{-1}\frac{1+m\sigma}{m+\sigma}\right] \quad \text{region II} \tag{21}$$

Equations (20) and (21) give the resultant u-velocity on the upper surface of OA. By equation (15) the value on the right side of OB is the same thing with opposite sign (with σ designating $\beta z/x$ instead of $\beta y/x$ as for OA).

The surface pressure is related to the velocity by equation (13). Thus pressure is obtained by multiplying the values in equations (20) and (21) by $-\rho V$.

Damping in roll. - The pressure distributions just determined for each of the two inner faces of the first quadrant (fig. 2) clearly contribute identical additive rolling moments. The total rolling moment for the cruciform is therefore eight times that contributed by the upper face of OA.

The local pressure on OA is proportional to Σu and by equations (20) and (21) Σu is of the form $x\,f(\sigma)$. For such a distribution calculation shows that the rolling moment contributed by this pressure is proportional to $\int_0^m \sigma f(\sigma)\,d\sigma$. The damping-in-roll coefficient for the complete cruciform is proportional to this integral and is given by

$$C_{l_p} = -\frac{2\beta}{m^3 p}\int_0^m \sigma f(\sigma)\,d\sigma$$

where the factor of eight mentioned previously has been taken into account. Upon substituting equations (20) and (21) and carrying out the integration, there results

$$C_{l_p} = -\frac{2m}{3\pi\beta(m^2-1)^2}\left(2m^2-5+\frac{2m^4-5m^2+6}{\sqrt{m^2-1}}\sec^{-1}m\right) \qquad (22)$$

Equation (22) gives the damping-in-roll coefficient for a cruciform delta wing with supersonic leading edges. For the case of sonic leading edges ($m = 1$) a limiting process yields

$$C_{l_p} = -\frac{88}{45\pi\beta} \qquad (23)$$

(This same result can be obtained with considerably less labor by limiting the foregoing analysis at the outset to the sonic-edge case.)

CRUCIFORM WITH SUBSONIC LEADING EDGES

The cross section of a single quadrant in a plane x = constant is shown in figure 5. The trace of the Mach cone from the apex is also shown. The wing panel traces are shown solid, and dotted-line extensions out to the Mach cone have been added. On the two wing panels the boundary conditions for rolling motion (angular velocity p) are $w = -py$ and $v = pz$, respectively. The dotted-line extensions carry no lift, and this condition can be specified by the relation $\Delta u = 0$, Δu being the jump in u across the dotted line. Finally the entire disturbance u,v,w must vanish on the Mach cone.

It is possible to satisfy these boundary conditions by means of a suitable distribution of doublets on the panels, the same on each panel. When the fourfold symmetry is taken into account, the u-velocity induced by these doublets at the dotted lines is seen to be zero. Thus the conditions $\Delta u = 0$ become $u = 0$. With this change then, the boundary conditions for adjacent quadrants are no longer interdependent and the flow in the typical quadrant (fig. 5) is completely determined by the conditions along its own boundary.

Figure 5 is redrawn with $u = 0$ in place of $\Delta u = 0$ and designated flow 6(a) in figure 6. Starting with this figure, the problem is further simplified by the principle of superposition. The flows specified as 6(b) and 6(c) will superpose to yield the flow specified as 6(a). Flow 6(c) can be seen to be a mirror image of flow 6(b) rotated through 90° with sign change. The problem for

the entire cruciform is thus reduced to the solution for the flow specified by the boundary conditions labeled flow 6(b).

Because of the difficulty of obtaining an exact solution, an iteration procedure was decided upon. The procedure is schematically represented by figure 7. The unknown u-velocity in the specifications for flows 7(a), 7(b), 7(c), . . . is to be solved for successively. The flows may then be superposed to converge to a solution for flow 6(b). Flow 7(a) clearly violates the requirement $u = 0$ in the vertical dotted region. Flow 7(b) attempts to rectify the situation by cancelling the velocity $u = u_B$ obtained in that region. In so doing, however, flow 7(b) leads to a much smaller induced u-velocity in the horizontal dotted region. This velocity $u = u_{A,b}$ is cancelled by flow 7(c), but at the cost of again slightly violating the condition $u = 0$ on the vertical dotted region, and so on.

If the dotted regions are relatively small (parameter m not too small compared with unity) the successive u-velocities in flows 7(a), 7(b), 7(c), . . . , will diminish rapidly, providing rapid convergence. It will be shown that the iteration process may be terminated after the evaluation of flow 7(b) with small loss in accuracy if $m \geq 0.5$; the velocities to be calculated are then u_A, u_B, $u_{B,b}$, and $u_{A,b}$.

Solution for u_A. - The vertical panel bounding flow 7(a) (fig. 7) completely isolates disturbances from the left and right sides, and the method of images is applicable, as for the supersonic-edge case. The same reasoning as for that case leads to figure 8, which is again a delta wing with linear twist, but this time with subsonic leading edges. The value of u on the right-hand panel of this wing (upper surface) is the desired value of u_A. The solution presents a problem in its own right, and the details are given in appendix B. (The solution was also obtained in reference 9 by a different method.) The result is given in equations (B2) and (B17):

$$u_A = \frac{2px}{3\pi\beta^2} \frac{a(m)+\delta^2 b(m)}{\sqrt{m^2-\delta^2}} \tag{24}$$

where

$$a(m) = \frac{3m^3(E-m^2K)}{(1-2m^2)E+m^2K}$$

$$b(m) = \frac{3m^3(K-E)}{(1-2m^2)E+m^2K}$$

and K and E are complete elliptic integrals of modulus $k = \sqrt{1-m^2}$.

Solution for u_B. - According to reference 10 the analytic continuation of a conical surface distribution of u, $u(\sigma)$ into space is obtained (subject to certain restrictions) by replacing σ by ζ and taking the real part. (See discussions in appendix B.) In the present case u_A is not conical, but $\partial u_A/\partial x$ is conical, and the procedure will apply to the latter. The equation for $\partial u_A/\partial x$ with ζ inserted is given in equation (B7). Along the z-axis (that is, along OB) ζ assumes the value $i\nu/\sqrt{1-\nu^2}$ where $\nu \equiv \beta z/x$. (See equation (B3).) With this value equation (B7) becomes

$$\left(\frac{\partial u}{\partial x}\right)_B = \frac{2p}{3\pi\beta^2} \frac{a\,m^2+e\nu^2}{\left[m^2+(1-m^2)\nu^2\right]^{3/2}} \sqrt{1-\nu^2}$$

where

$$e \equiv (2-m^2)a + m^2b$$

The integration with respect to x then yields

$$u_B = \frac{2px}{3\pi\beta^2} f_B(\nu)$$

where

$$f_B(\nu) \equiv \nu\left[a\left(-F(\phi,k) + \frac{\sqrt{1-\nu^2}}{\nu\sqrt{m^2+k^2\nu^2}}\right) + \frac{a+b}{k^2}\left(E(\phi,k) - m^2F(\phi,k) - \frac{k^2\nu\sqrt{1-\nu^2}}{\sqrt{m^2+k^2\nu^2}}\right)\right] \tag{25}$$

and

$$\phi = \cos^{-1}\nu$$

$$k = \sqrt{1-m^2}$$

(This expression reduces to the simple equation (19) when the leading edges are sonic, upon applying a limiting process as $m \to 1$.) The variation of u_B with ν is shown in figure 9 for $m = 0.866$.

Solution for $u_{B,b}$. - Refer again to flow 7(b) (fig. 7). The condition $w = 0$ along the horizontal axis permits the use of reflection in this axis. Thus $u_{B,b}$ is the value of u on the right-hand panel (lower surface) of the wing shown in figure 10. The exact solution of this wing presents an almost insuperable problem, and even a close approximation (for example, by the method of reference 11) is unduly laborious. The average magnitude of $u_{B,b}$ can be anticipated, however, to be small enough compared with u_B and u_A so that some inaccuracy may be tolerated. Accordingly, in place of the exact $u_{B,b}$ a relatively easily calculated flow will be used that fails to cancel u_B exactly for $\nu \geq n$, but does cancel it on the average.

This approximate distribution $u_{B,b}$ may be specified with the aid of figure 10 with z replaced by y and upper and lower surfaces interchanged for convenience. This flow consists of the superposition of four flows, (1), (2), (3), and (4), determined by the following respective boundary conditions at the wing surface:

(1)	$-1 \leq \nu \leq 1$	$w = -\kappa x$
(2)	$-1 \leq \nu \leq 1$	$w = +\kappa\beta\lvert y\rvert$
(3)	$-m \leq \nu \leq m$	$w = \kappa x$
	$m < \lvert\nu\rvert \leq 1$	$u = 0$
(4)	$-m \leq \nu \leq m$	$w = -\kappa\beta\lvert y\rvert$
	$m < \lvert\nu\rvert \leq 1$	$u = 0$

It is clear that the superposition of these flows satisfies the required boundary condition for $u_{B,b}$ that $w = 0$ in the region $-m \leq \nu \leq m$. In addition, there will be a nonvanishing quasi-conical distribution of u in the regions $m < \nu \leq 1$ from flows (1) and (2), although flows (3) and (4) contribute nothing there.

Flows (1) and (3) may be recognized as corresponding to the pitching delta wing with sonic and subsonic leading edges, respectively. Flows (2) and (4) correspond to the delta wing with linear twist, again with sonic and subsonic leading edges, respectively. The solutions for (1) and (3) are well-known (reference 12) and those for (2) and (4) have already been obtained herein. The solutions for the u-velocities are

$$u_1 = \frac{4\kappa x}{3\pi\beta} \frac{2-\nu^2}{\sqrt{1-\nu^2}}$$

$$u_2 = \frac{-2\kappa x}{3\pi\beta} \frac{1+\nu^2}{\sqrt{1-\nu^2}}$$

$$u_3 = \frac{-2\kappa x}{3\pi\beta} \frac{a_1(m)+\nu^2 b_1(m)}{\sqrt{m^2-\nu^2}}$$

$$u_4 = \frac{2\kappa x}{3\pi\beta} \frac{a(m)+\nu^2 b(m)}{\sqrt{m^2-\nu^2}}$$

where $a_1(m)$, $b_1(m)$, $a(m)$, and $b(m)$ are defined in appendix A. Note that u_3 and u_4 are to be taken equal to zero for $\nu > m$.

The sum $u_1 + u_2 + u_3 + u_4$ is the tentative approximation to $u_{B,b}$. This sum is

$$u_{B,b} = \frac{2\kappa x}{\pi\beta}\left[\sqrt{1-\nu^2} - \frac{A(m)+\nu^2 B(m)}{3\sqrt{m^2-\nu^2}}\right] \qquad -m < \nu < m \qquad (26a)$$

$$= \frac{2\kappa x}{\pi\beta}\sqrt{1-\nu^2} \qquad m < |\nu| \leq 1 \qquad (26b)$$

where

$$A(m) \equiv a_1(m) - a(m)$$

$$B(m) \equiv b_1(m) - b(m)$$

and the parameter κ is yet to be determined.

In the region $m < |\nu| \leq 1$, $u_{B,b}$ is given by equation (26b). The variation with ν is shown graphically in figure 11 for a selected value of κ. On the same figure is shown a portion of the variation of u_B with ν for $m = 0.866$. The value of was chosen to make $u_{B,b} = -0.8\ u_B$ at $\nu = m+$. This value is, by virtue of equations (25) and (26b),

$$\kappa = \frac{0.8\ f_B(m)}{3\sqrt{1-m^2}}\frac{p}{\beta} = \frac{-0.8\ f_B(m)}{3k}\frac{p}{\beta} \qquad (26c)$$

where $f_B(m)$ is $f_B(\nu)$ (equation (25)) with $\nu = n$. This selection of κ does not effect an exact average cancellation of u_B by $u_{B,b}$ in the range $m < |\nu| \leq 1$; instead, the ordinates near $\nu = m$ are given more weight as suggested by equation (17a) of reference 11. It is thought that the average of $u_{B,b}$ calculated in this way over the range $0 \leq \nu \leq m$ is within ± 25 percent of the exact value.

Solution for $u_{A,b}$. - The distribution $u_{A,b}$ along the y-axis (fig. 7(b)) is obtained by analytic continuation of the distribution $u_{B,b}$, which is known along the z-axis. The procedure is patterned after that discussed in the solution for u_B. The result is obtained without difficulty as

$$u_{A,b} = \frac{2\kappa x}{\pi\beta}\left\{\sqrt{1-\sigma^2} - \sigma\cos^{-1}|\sigma| - \frac{\sigma}{3}\left[\frac{A}{m^2}\left(m^2F(\phi,k) - 2E(\phi,k) + \frac{(m^2+2k^2\sigma^2)\sqrt{1-\sigma^2}}{\sqrt{m^2+k^2\sigma^2}}\right) + \frac{e_1}{m^2k^2}\left(E(\phi,k) - m^2F(\phi,k) - \frac{k^2\sigma\sqrt{1-\sigma^2}}{\sqrt{m^2+k^2\sigma^2}}\right)\right]\right\} \qquad (27)$$

where

$$e_1 = (2-m^2)\ A + m^2B$$

Resultant u-velocity and pressure distribution. - The unknown surface u-velocity distribution in the flow defined by figure 6(b) has now been determined to the desired accuracy. The value on the

upper surface of OA is $u_A(\sigma)$ (equation (24)) plus $u_{A,b}(\sigma)$ (equation (27)); the value on the right-hand side of OB is $u_B(\nu)$ (equation (25)) plus $u_{B,b}(\nu)$ (equations (26a) to (26c)). To the flow of figure 6(b) must be added the mirror-image flow with reversed sign defined by figure 6(c). This image flow is characterized by a u-velocity $-u_A(\nu)$ $-u_{A,b}(\nu)$ along OB and a u-velocity $-u_B(\sigma)$ $-u_{B,b}(\sigma)$ along OA. Superposition yields the resultant values:

$$\Sigma u \equiv (\Sigma u)_A = u_A(\sigma) - u_B(\sigma) - u_{B,b}(\sigma) + u_{A,b}(\sigma) \qquad (28)$$

along the upper surface of OA, and

$$\Sigma u \equiv (\Sigma u)_B = -\left[u_A(\nu) - u_B(\nu) - u_{B,b}(\nu) + u_{A,b}(\nu)\right] \qquad (29)$$

along the right-hand side of OB.

The surface pressure distribution (deviation from stream pressure) is obtained by multiplying the values of Σu by $-\rho V$, according to the linearized Bernoulli equation (13).

Damping in Roll

The pressure distributions just determined for each of the two inner faces of a quadrant of the cruciform contribute identical additive rolling moments; this is a consequence of the antisymmetry of equations (28) and (29). The total rolling moment for the cruciform is therefore eight times that contributed by the upper surface of OA.

The local pressure on OA is proportional to Σu, and the equations show that each of the components of Σu is of the form $xf_1(\sigma)$. For each such component the contribution to the damping-in-roll coefficient for the entire cruciform was earlier pointed out to be

$$\Delta_1 C_{l_p} = \frac{-2\beta}{m^3 p} \int_0^m \sigma f_1(\sigma)\, d\sigma$$

Thus the total value of C_{l_p} is

$$C_{l_p} = \Delta_A C_{l_p} + \Delta_B C_{l_p} + \Delta_{B,b}\, C_{l_p} + \Delta_{A,b}\, C_{l_p} \tag{30a}$$

the increments corresponding respectively to u_A, $-u_B$, $-u_{B,b}$ and $u_{A,b}$. Upon carrying out the integrations there is obtained

$$\Delta_A C_{l_p} = -\frac{4}{9\pi\beta m^3}\left[3ma + 2m^3 b\right] \tag{30b}$$

$$\Delta_B C_{l_p} = \frac{4}{9\pi\beta m^3}\left[m^2 f_B(m) + \frac{m}{k^2}\left(1 - \frac{k}{\sqrt{1+k^2}}\right)\left(a - \frac{3e}{2k^2}\right) + \frac{em}{2k\sqrt{1+k^2}} - \frac{\sin^{-1} k - \sin^{-1} k^2}{k^3}\left(am^2 - \frac{(3-2k^2)e}{2k^2}\right)\right] \tag{30c}$$

$$\Delta_{B,b}\, C_{l_p} = \frac{4}{9\pi\beta m^3}\,\frac{0.8\, f_B(m)}{k}\left[mA + \frac{2}{3}\, m^3 B + k^3 - 1\right] \tag{30d}$$

$$\Delta_{A,b}\, C_{l_p} = \frac{4}{9\pi\beta m^3}\,\frac{0.8 f_B(m)}{3k}\left\{1+3k-4k^3-3m^3 \cos^{-1} m - m^2 f_{A,b}(m) - \frac{e_1 m}{2k\sqrt{1+k^2}} - \frac{m}{k^2}\left(1 - \frac{k}{\sqrt{1+k^2}}\right)\left(A - \frac{3e_1}{2k^2}\right) + \frac{\sin^{-1} k - \sin^{-1} k^2}{k^3}\left[Am^2 - \frac{(3-2k^2)e_1}{2k^2}\right]\right\} \tag{30e}$$

where a, b, e, A, B, and e_1 are functions of m defined in appendix A; the function $f_B(m)$ has been evaluated from $f_B(\nu)$ in equation (25)

$$f_B(m) = \frac{a}{m}\left(-m^2 F(\phi_1,k) + \frac{k}{\sqrt{1+k^2}}\right) + \frac{m(a+b)}{k^2}\left(-m^2 F(\phi_1,k) + E(\phi_1,k) - \frac{k^3}{\sqrt{1+k^2}}\right) \quad (30f)$$

where

$$\phi_1 = \sin^{-1} k$$

and $f_{A,b}(m)$ is $f_B(m)$ with A in place of a and B in place of b.

The variation of $-C_{l_p}$ with m according to equations (30a) to (30f) has been plotted in figure 12. On the same figure the successive contributions of the iteration process, $\Delta_A C_{l_p}$, $\Delta_B C_{l_p}$, $\Delta_{B,b} C_{l_p}$, and $\Delta_{A,b} C_{l_p}$ are shown. It is seen that the sum $\Delta_{B,b} C_{l_p}$ plus $\Delta_{A,b} C_{l_p}$ reaches only 4.7 percent of C_{l_p} as m is reduced to 0.5 and thus justifies the roughness of the approximation for $u_{B,b}$ and $u_{A,b}$. The estimated ±25-percent uncertainty in the average value of $u_{B,b}$ and $u_{A,b}$ (which is surely liberal) accordingly contributes only ±1.2-percent uncertainty to C_{l_p} at m = 0.5.

A plot of $u_{A,b}$ (not shown) shows a general similarity to that for u_B (fig. 9). From this similarity the contribution to C_{l_p} of the next iteration, flow 7(c) of figure 7, with velocity components $u_{A,c}$ and $u_{B,c}$, can be roughly estimated. The proportion contributed is according to this estimation:

$$\frac{\Delta_{A,c} C_{l_p} + \Delta_{B,c} C_{l_p}}{C_{l_p}} \cong \left(\frac{-u_{A,b}(0)}{u_B(0)}\right)\left(\frac{\Delta_{B,b} C_{l_p} + \Delta_{A,b} C_{l_p}}{C_{l_p}}\right)$$

This ratio increases with decreasing m; for m = 0.5 the value is (0.025)(-0.047) = -0.0012, or a little over -0.1 percent. Thus

above $m = 0.5$ the total contribution of flow 7(c) is small compared with the uncertainty (±1.2 percent of C_{l_p} at $m = 0.5$) in the contribution of flow 7(b). For this reason flow 7(c) and further iterations have been neglected in the computation of C_{l_p}.

Examination of figure 12 in the light of the foregoing considerations shows that the estimated uncertainty in C_{l_p} increases progressively from zero at $m = 1$ as m is decreased. The graphs are terminated at $m = 0.5$ where the error reaches an estimated ±1.2 percent +0.1 percent.

DISCUSSION AND CONCLUDING REMARKS

In the preceding three sections, the damping in roll for the cruciform delta wing has been evaluated for three speed regimes characterized by three ranges of the edge-slope Mach number parameter m. Equation (9) (rigorous for $m \to 0$) is considered to be a good approximation for $0 < m \leq 0.25$. Equation (30) was shown to be a good approximation (progressively better with increasing m) for $0.5 \leq m \leq 1$. Finally, equation (22) is exact for $1 \leq m \leq \infty$. (Both equations (22) and (30) reduce to equation (23) for $m = 1$.)

The variation of $-\beta C_{l_p}$ with m from these three equations is plotted in figure 13. It is seen that equation (30) appears to be asymptotic to the slender-wing-theory result (equation (9)) for decreasing m. In fact, a satisfactory interpolation (shown dotted) in the neglected range $0.25 \leq m \leq 0.5$ is indistinguishable from equation (9).

The damping in roll of a multiplanar delta wing of N panels is always less than $N/2$ times the damping of the plane delta wing of two panels. The reduction is caused by interference between the panels in different planes. The present results show that the loss for the cruciform delta varies from 19 percent as $m \to 0$ to 7 percent at $m = 1$ and decreases to zero as $m \to \infty$. For $m \to 0$, the interference loss increases progressively with the number of panels as follows: three panels, 10 percent; four panels, 19 percent; infinite number of panels, 100 percent. The relative total damping in roll for $m \to 0$ is: two panels, 100 percent (standard of comparison); three panels, 135 percent; four panels, 162 percent; infinite number of panels, 400 percent. Finally, the

damping in roll for an infinite number of panels, regardless of aspect ratio, is independent of Mach number both below and above the speed of sound.

Lewis Flight Propulsion Laboratory,
National Advisory Committee for Aeronautics,
Cleveland, Ohio, August 24, 1950.

APPENDIX A

SYMBOLS

The following symbols are used in this report:

$A = A(m) = a_1(m) - a(m)$

$a = a(m) = \dfrac{3m^3(E(k)-m^2K(k))}{(1-2m^2)E(k)+m^2K(k)}$

$a_1 = a_1(m) = \dfrac{3\pi m^2k^2}{(1-2m^2)E(k)+m^2K(k)}$

$B = B(m) = b_1(m) - b(m)$

$b = b(m) = \dfrac{3m^3(K(k)-E(k))}{(1-2m^2)E(k)+m^2K(k)}$

$b_1 = b_1(m) = \dfrac{-3\pi k^2/2}{(1-2m^2)E(k)+m^2K(k)}$

C_{l_p} damping-in-roll derivative $= \dfrac{\text{rolling moment}}{\frac{1}{2}\rho V^2 \cdot \text{area two panels} \frac{ps}{V}}$

cn t, sn t, dn t Jacobian elliptic functions

$E = E(k)$ complete elliptic integral of second kind, modulus k

$E(\phi,k)$ incomplete elliptic integral of second kind, modulus k, amplitude ϕ

$e = e(m) = (2-m^2)\,a(m) + m^2b(m)$

$e_1 = e_1(m) = (2-m^2)\,A(m) + m^2B(m)$

$F(\phi,k)$	incomplete elliptic integral of first kind, modulus k, amplitude ϕ
$f(\sigma)$	function of σ (different definitions in different places)
$f_{A,b}(m)$	$f_B(m)$ with A in place of a and B in place of b
$f_B(m)$	$\left[f_B(\nu)\right]_{\nu=m}$ given by equation (30f)
$f_B(\nu)$	defined in equation (25)
I	moment of inertia
i	$\sqrt{-1}$
K	function related to $\Delta\phi$ defined in equation (1)
K(k)	complete elliptic integral of first kind, modulus k
$k=\sqrt{1-m^2}$	modulus of elliptic integrals
L	rolling moment, positive in sense of a right-hand screw proceeding upstream
M	Mach number = $\frac{\text{flight speed}}{\text{sonic speed}}$
m	value σ at right edge of delta wing $\left(\frac{\tan\epsilon}{\tan\mu}\right)$
N	number of panels (half-deltas) in multiplanar wing (N = 4 for cruciform)
P	local pressure minus stream pressure
p	angular rolling velocity, positive in sense of a right-hand screw proceeding upstream
q	angular pitching velocity, positive in sense of a right-hand screw proceeding outward along y-axis
Re	real part of

r	radial distance from x-axis
s	semispan
t	argument of elliptic functions $(=F(\phi,k))$
$U(\zeta)$	function of complex parameter ζ
u, v, w	disturbance velocity components along x-, y-, z-axes, respectively
V	free-stream velocity (flight speed)
x, y, z	Cartesian coordinates: x-axis parallel to free-stream direction; y-axis horizontal and toward right, looking upstream; z-axis vertically upward
β	$\sqrt{M^2-1}$
Γ	circulation
$\Gamma(N)$	gamma function (equation 481, reference 14)
Δ	increment in
ϵ	$\frac{\beta y+i\beta z}{x+\sqrt{x^2-\beta^2y^2-\beta^2z^2}}$; also semivertex angle of delta plan form
ζ	$\frac{2\epsilon}{1+\epsilon^2}$, complex conical ray parameter
θ	parameter defining r (defined differently in equations (1), (2), and (6))
κ	constant
μ	Mach angle $\left(=\sin^{-1}\frac{1}{M}\right)$
ν	$\beta z/x$
ρ	gas density

σ	$\beta y/x$ except where designated otherwise
τ	dummy variable used in limiting process
ϕ	velocity potential; also amplitude of elliptic integrals

Subscripts:

A	along OA (upper surface)
A,b	along OA (upper surface), contribution of flow 7(b)
A,c	along OA (upper surface), contribution of flow 7(c)
B	along OB (right-hand side)
B,b	along OB (right-hand side), contribution of flow 7(b)
B,c	along OB (right-hand side), contribution of flow 7(c)
i	dummy index
L.E.	along leading edge
x	$\frac{\partial}{\partial x}$
y	$\frac{\partial}{\partial y}$
z	$\frac{\partial}{\partial z}$
l	running variable
1, 2, 3, 4	distinguishing subscripts
I	in region I
II	in region II

APPENDIX B

DELTA WING WITH SYMMETRIC LINEAR TWIST

(SUBSONIC LEADING EDGES)

The loading on a delta wing with symmetric linear spanwise variation of angle of attack is easily obtained when the leading edges are supersonic. The result is given in equations (16) and (17), upon multiplication by $-\rho V$. The difficulty is increased considerably when the leading edges are subsonic. The subsequent derivation applies to this subsonic case.

The procedure employs the development of Busemann's complex-variable method for conical flows presented in reference 10. The starting point is an assumed function for the distribution of u with two undetermined parameters a and b. The procedure of reference 10 can then be applied to obtain a value of $\partial w/\partial x$ in terms of a and b, and then again to obtain $\partial w/\partial y$ in terms of a and b. Insertion of the condition for linear twist $(w = -p|y|)$ requires that $\partial w/\partial x = 0$ and $\partial w/\partial y = \mp p$. The simultaneous solution of these two equations for a and b completes the solution for u.

The proper form for the assumed function for u was arrived at partly from the requirements of reference 10 and partly from a consideration of the asymptotic form assumed by equation (17) when the leading edges are sonic $(m = 1)$. A limiting process for the sonic case yields

$$u = \frac{2px}{3\pi\beta^2} \frac{1+\sigma^2}{\sqrt{1-\sigma^2}} \tag{B1}$$

Comparison of this result with the known u-velocity for a pitching delta wing for $m = 1$ and for $m < 1$ suggests the generalization

$$u = \frac{2px}{3\pi\beta^2} \frac{a(m)+\sigma^2\, b(m)}{\sqrt{m^2-\sigma^2}} \tag{B2}$$

for the present wing for $m \leq 1$. Other considerations, omitted for brevity, support the choice. Equation (B2) will reduce to (B1) when $m = 1$ if $a(1) = b(1) = 1$.

The relevant part of the conical-flow theory of reference 10 is briefly as follows: It is proved that any function of the complex parameter

$$\left.\begin{aligned} \zeta &\equiv \frac{2\epsilon}{1+\epsilon^2} \\ \text{where} \\ \epsilon &\equiv \frac{\beta y + i\beta z}{x + \sqrt{x^2 - \beta^2 y^2 - \beta^2 z^2}} \end{aligned}\right\} \tag{B3}$$

gives a value of u that is conical and consistent with the Prandtl-Glauert equation (12). This value of u - call it $U(\zeta)$ - is complex in general, and both the real and the imaginary parts separately satisfy equation (12). Furthermore, the value of w associated with $u = \operatorname{Re} U$ may be obtained from the relation

$$w(\zeta) = -\operatorname{Re} i\beta \int_{\zeta=1}^{\zeta} \frac{\sqrt{1-\zeta^2}}{\zeta}\, dU \tag{B4}$$

For $z = 0$ the parameter ζ reduces to $\beta y/x \equiv \sigma$. Thus by the foregoing principle a suitable known or assumed conical surface distribution of $u, f(\zeta)$ may be analytically continued off the surface as a spatial distribution by replacing σ by ζ and taking the real part. Either the surface or spatial value of w associated with this distribution of u may then be obtained from equation (B4).

In the present application, the requirement that u be conical (function of σ alone) is not met by equation (B2); the velocity gradients u_x and u_y are, however, conical:

$$u_x = \frac{2p}{3\pi\beta^2} \frac{am^2 - (2a+m^2b)\sigma^2}{(m^2-\sigma^2)^{3/2}} \tag{B5}$$

$$u_y = \frac{2p}{3\pi\beta} \frac{(a+2m^2b)\sigma - b\sigma^3}{(m^2-\sigma^2)^{3/2}} \tag{B6}$$

The variables u_x, v_x, w_x may in this case replace u, v, w, respectively, in the method of reference 10. Alternatively u_y, v_y, w_y may replace u, v, w. These substitutions are easily justified by differentiating the Prandtl-Glauert equation (12) and employing the irrotationality conditions ($v_x = u_y$, . . .).

The analytic continuation of equations (B5) and (B6) is thus obtained by the substitution of ζ for σ:

$$u_x(\zeta) = \mathrm{Re}\ U_x = \mathrm{Re}\ \frac{2p}{3\pi\beta^2} \frac{am^2-(2a+bm^2)\zeta^2}{(m^2-\zeta^2)^{3/2}} \tag{B7}$$

$$u_y(\zeta) = \mathrm{Re}\ U_y = \mathrm{Re}\ \frac{2p}{3\pi\beta} \frac{(a+2m^2b)\zeta-b\zeta^3}{(m^2-\zeta^2)^{3/2}} \tag{B8}$$

Also, the following equations correspond to equation (B4):

$$w_x(\zeta) = -\mathrm{Re}\ i\beta \int_{\zeta=1}^{\zeta} \frac{\sqrt{1-\zeta^2}}{\zeta}\, dU_x \tag{B9}$$

$$w_y(\zeta) = -\mathrm{Re}\ i\beta \int_{\zeta=1}^{\zeta} \frac{\sqrt{1-\zeta^2}}{\zeta}\, dU_y \tag{B10}$$

In the plane $\zeta = \sigma$, U_x and U_y are seen to be wholly real in the ranges $-m < \sigma < 0$, $0 < \sigma < m$. Equations (B9) and (B10) then show that w_x and w_y must be constant in these ranges. A discontinuity in w_y may, however, occur in crossing (an infinitesimal distance above) the origin because the odd powers of ζ in equation (B8) become imaginary there. This behavior is consistent with the desired boundary conditions already discussed:

$$\begin{aligned} w_x &= 0 && -m < \sigma < m \\ w_y &= p && -m < \sigma < 0 \\ &= -p && 0 < \sigma < m \end{aligned} \tag{B11}$$

It is convenient; and according to the foregoing discussion it will suffice, then, to evaluate equation (B9) for w_x at $\sigma = m-$ and equation (B10) for w_y at $\sigma = m-$ and at $\sigma = -m+$. A limiting process must be used, including an approach from slightly above the y-axis ($z \neq 0$) because of the singularity at $\sigma = \pm m$. (The procedure is mathematically equivalent to taking the "finite part" as done by Hadamard (reference 13).) Equation (B9) thus becomes

$$w_x(m-) = \lim_{\tau \to 0} \left(\lim_{\nu \to 0} -\mathrm{Re}\ i\beta \int_{\zeta=1}^{m-\tau+i\nu} \frac{\sqrt{1-\zeta^2}}{\zeta}\, dU_x \right) \tag{B12}$$

and similarly for equation (B10).

The integrations are most easily evaluated with the aid of the following elliptic-function substitutions, together with the tables of integrals in references 14 and 15:

$$\sqrt{1-\zeta^2} = k\ \mathrm{sn}\ t$$

$$\sqrt{\zeta^2-m^2} = k\ \mathrm{cn}\ t$$

$$\zeta = \mathrm{dn}\ t$$

$$d\zeta = -k^2\ \mathrm{sn}\ t\ \mathrm{cn}\ t\ dt$$

where

$$\begin{aligned} t &= F(\phi,k) \\ \phi &= \sin^{-1}\sqrt{\frac{1-\zeta^2}{1-m^2}} \\ k &= \sqrt{1-m^2} \end{aligned} \tag{B13}$$

The evaluation of equations (B9) and (B10) by use of the limiting process of equation (B12) yields

$$w_x\ (m-) = \frac{-2p}{3\pi\beta} \frac{1}{1-m^2} \left[(a+m^2b)K(k) - (a+b)E(k) \right] \tag{B14}$$

$$w_y(m-) = \frac{-2p}{3\pi} \frac{a+2m^2b}{m^3} \frac{\pi}{2} \tag{B15a}$$

and changing the upper limit to $-m+\tau+i\upsilon$

$$w_y(-m+) = +\frac{2p}{3\pi}\frac{a+2m^2b}{m^3}\frac{\pi}{2} \tag{B15b}$$

The left-hand sides of these three equations are now evaluated by means of equations (B11). Equations (B15a) and (B15b) lead to the same equation, and there result but two simultaneous equations for a and b:

$$\left.\begin{aligned} 0 &= \frac{-2p}{3\pi\beta}\frac{1}{1-m^2}\left[(a+m^2b)K - (a+b)E\right] \\ -p &= \frac{-2p}{3\pi}\frac{a+2m^2b}{m^3}\frac{\pi}{2} \end{aligned}\right\} \tag{B16}$$

The solution of equations (B16) is

$$\left.\begin{aligned} a = a(m) &= \frac{3m^3(E-m^2K)}{(1-2m^2)E+m^2K} \\ b = b(m) &= \frac{3m^3(K-E)}{(1-2m^2)E+m^2K} \end{aligned}\right\} \tag{B17}$$

The values of a(m) and b(m) just obtained are to be substituted in equation (B2). This completes the solution for the distribution of u-velocity (proportional to pressure) for the delta wing with linear symmetric twist and subsonic leading edges.

A slight modification of the foregoing procedure yields the known pressure distribution for a pitching delta wing in a very simple manner. The boundary conditions (equation (B11)) are merely replaced by $w_x = -p/\beta$ and $w_y = 0$. With these values, equations (B14) and (B15) lead at once to the correct values of a and b for a wing pitching with angular velocity $q = p/\beta$. These are the values $a_1(m)$ and $b_1(m)$, respectively, obtained from reference 12, expressions for which are given in appendix A.

A natural question arises; namely, whether the procedure of this appendix could be used to solve the main problem of the rotating cruciform with subsonic leading edges because the form of the

pressure-distribution function might be guessed from the supersonic-edge case in the limit as $m \longrightarrow 1$. If this method were capable of successful application, the exact solution rather than an approximate one would be expected. Unfortunately, there are certain difficulties. First, the pressure distribution is known for the other limiting case $m \longrightarrow 0$, and the functional form is quite different. Therefore the functional form for intermediate values of m cannot be guessed with confidence. Second, in the contemplated application the analytic continuation of the pressure distribution would require that $U(\zeta)$ possess an imaginary part, the evaluation of which may offer considerable difficulty. This can be seen as follows: Associate the function $U_1(\zeta)$ with the horizontal panels and $U_2(\zeta)$ with the vertical panels. Call the corresponding induced velocities at the horizontal panels $w_1(x,y)$ and $w_2(x,y)$, respectively. Then the boundary condition may be stated as $w_1(x,y) + w_2(x,y) = -py$. Thus, because of w_2, the gradients $\partial w_1/\partial x$ and $\partial w_1/\partial y$ will undoubtedly fail to be constants; this can occur only if $U_1(\zeta)$ possesses a suitable imaginary part for $-m \leq \zeta = \sigma \leq m$. (See equations (B9) and (B10) and the discussion thereafter.)

REFERENCES

1. Spreiter, John R.: Aerodynamic Properties of Cruciform-Wing and Body Combinations at Subsonic, Transonic, and Supersonic Speeds. NACA Rep. 962, 1949. (Formerly NACA TN 1897.)

2. Jones, Robert T.: Properties of Low-Aspect-Ratio Pointed Wings at Speeds below and above the Speed of Sound. NACA Rep. 835, 1946. (Formerly NACA TN 1032.)

3. Westwater, F. L.: Some Applications of Conformal Transformations to Airscrew Theory. Proc. Cambridge Phil. Soc., vol. 32, pt. 4, Oct. 1936, pp. 676-684.

4. Bleviss, Zegmund O.: Some Roll Characteristics of Cruciform Delta Wings at Supersonic Speeds. Paper presented at Ann. Meeting I.A.S. (Los Angeles), July 12, 1950.

5. Ribner, Herbert S.: A Transonic Propeller of Triangular Plan Form. NACA TN 1303, 1947.

6. Harmon, Sidney M., and Jeffreys, Isabella: Theoretical Lift and Damping in Roll of Thin Wings with Arbitrary Sweep and Taper at Supersonic Speeds. Supersonic Leading and Trailing Edges. NACA TN 2114, 1950.

7. Moeckel, W. E., and Evvard, J. C.: Load Distributions Due to Steady Roll and Pitch for Thin Wings at Supersonic Speeds. NACA TN 1689, 1948.

8. Evvard, John C.: Theoretical Distribution of Lift on Thin Wings at Supersonic Speeds (An Extension). NACA TN 1585, 1948.

9. Goodman, Theodore R.: The Lift Distribution on a Delta Wing with Linear Twist. Rep. No. CAL/OM-524, Cornell Aero. Lab., Inc., Feb. 1949. (Rev., May 1949.) (Bur. Ord. Contract NOrd-10057.)

10. Jones, Robert T.: The Use of Conical and Cylindrical Fields in Supersonic Wing Theory. Compilation of Papers Presented at NACA-Univ. Conference on Aerodynamics (Langley Field, Va.), June 1948, pp. 341-353. (Reprinted by Durand Reprinting Comm. (C.I.T.), July 1948.)

11. Mirels, Harold: Lift-Cancellation Technique in Linearized Supersonic-Wing Theory. NACA TN 2145, 1950.

12. Brown, Clinton E., and Adams, Mac C.: Damping in Pitch and Roll of Triangular Wings at Supersonic Speeds. NACA Rep. 892, 1948. (Formerly NACA TN 1566.)

13. Hadamard, Jacques: Lectures on Cauchy's Problem in Linear Partial Differential Equations. Yale Univ. Press, 1923.

14. Peirce, B. O.: A Short Table of Integrals. Ginn and Co., 3d ed., 1929, p. 72.

15. Jahnke, Eugene, and Emde, Fritz: Tables of Functions. Dover Pub., 4th ed., 1945, pp. 96-97.

16. Lock, C. N. H., and Yeatman, D.: Tables for Use in an Improved Method of Airscrew Strip Theory Calculation. R. & M. No. 1674, British A.R.C., Oct. 1934.

TABLE I - VARIATION OF $N\Delta\phi/s^2p$ WITH r/s FOR LOW-ASPECT-RATIO MULTIPLANAR DELTA-WING CONFIGURATIONS OF 3 AND 4 PANELS

r/s	0.3	0.45	0.6	0.7	0.75	0.8	0.85	0.9	0.95	1.00
Four panels $N\Delta\phi/s^2p$ (cruciform)	0.710	1.176	1.540	1.672	1.686	1.657	1.566	1.384	1.066	0
Three panels $N\Delta\phi/s^2p$	0.671	1.067	1.298	1.395	1.385	1.335	1.235	1.115	0.851	0

For three panels the value of K at r/s = 0.85 given as 0.227 in reference 3 is clearly in error. Comparison with the approximate value 0.278 in reference 16 suggests that 0.272 was probably intended; the value $N\Delta\phi/s^2p = 1.235$ above corresponds to K = 0.272.

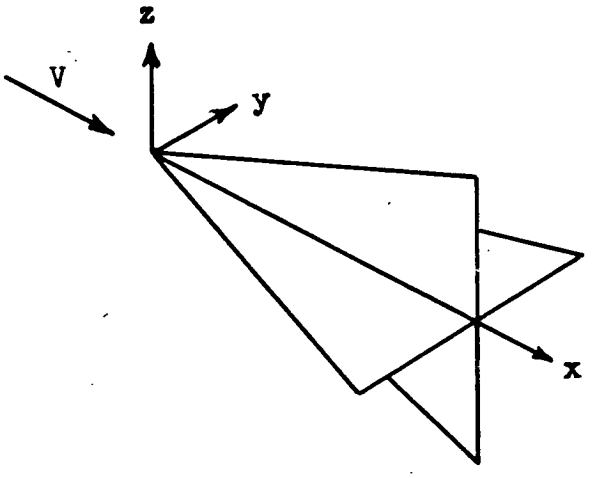

(a) Cruciform delta wing.

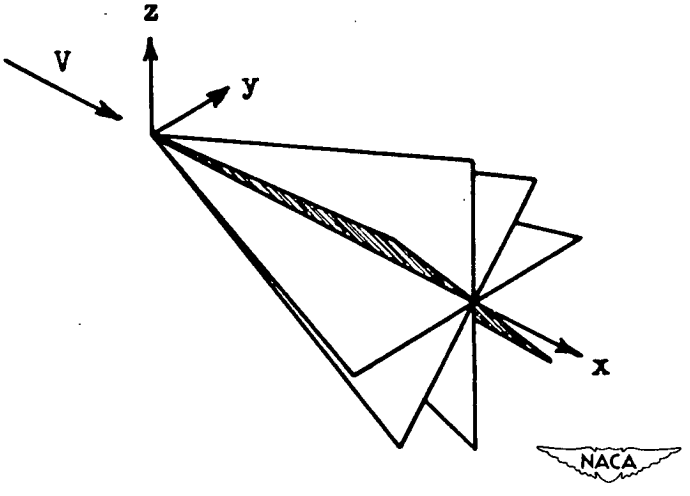

(b) Multiplanar delta wing.

Figure 1. - Delta wings and coordinate axes.

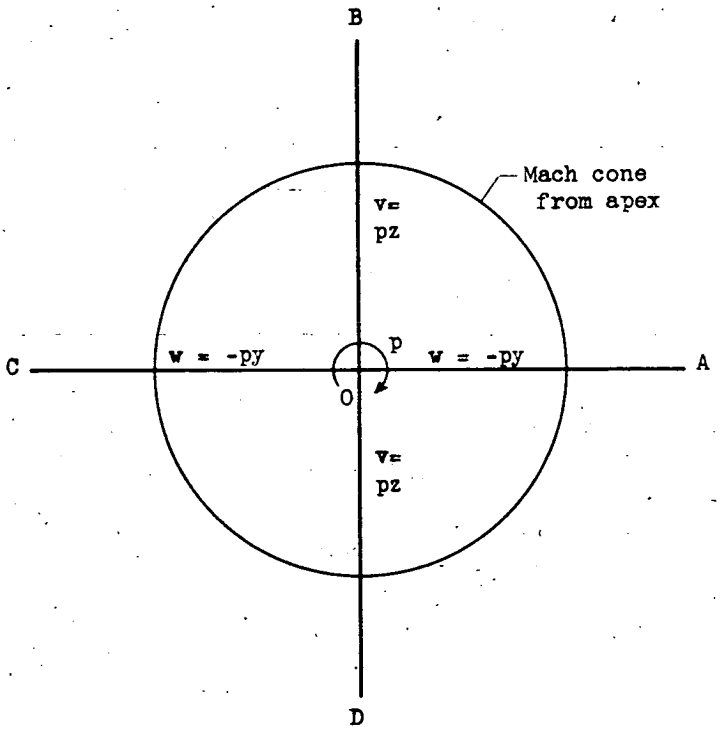

Figure 2. - Boundary conditions for rolling cruciform delta with supersonic leading edges. Section x = constant.

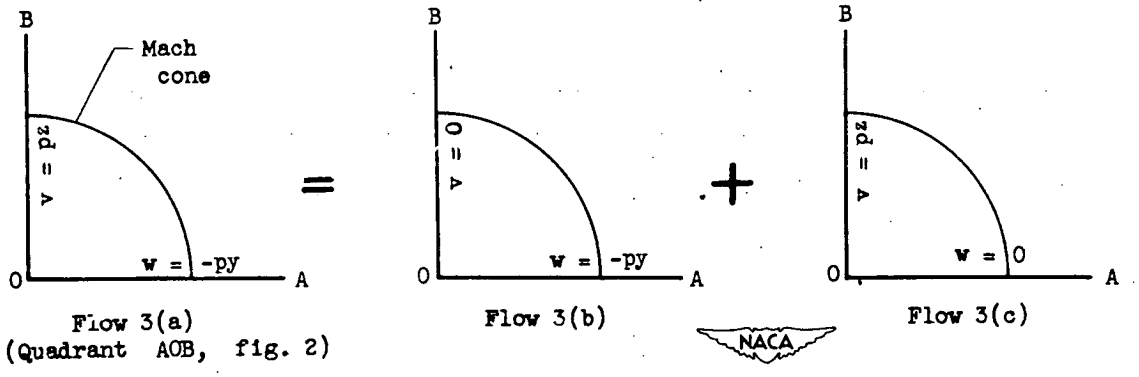

Flow 3(a)
(Quadrant AOB, fig. 2)

Flow 3(b)

Flow 3(c)

Figure 3. - Superposition of simpler flows to obtain flow in quadrant AOB of figure 2.

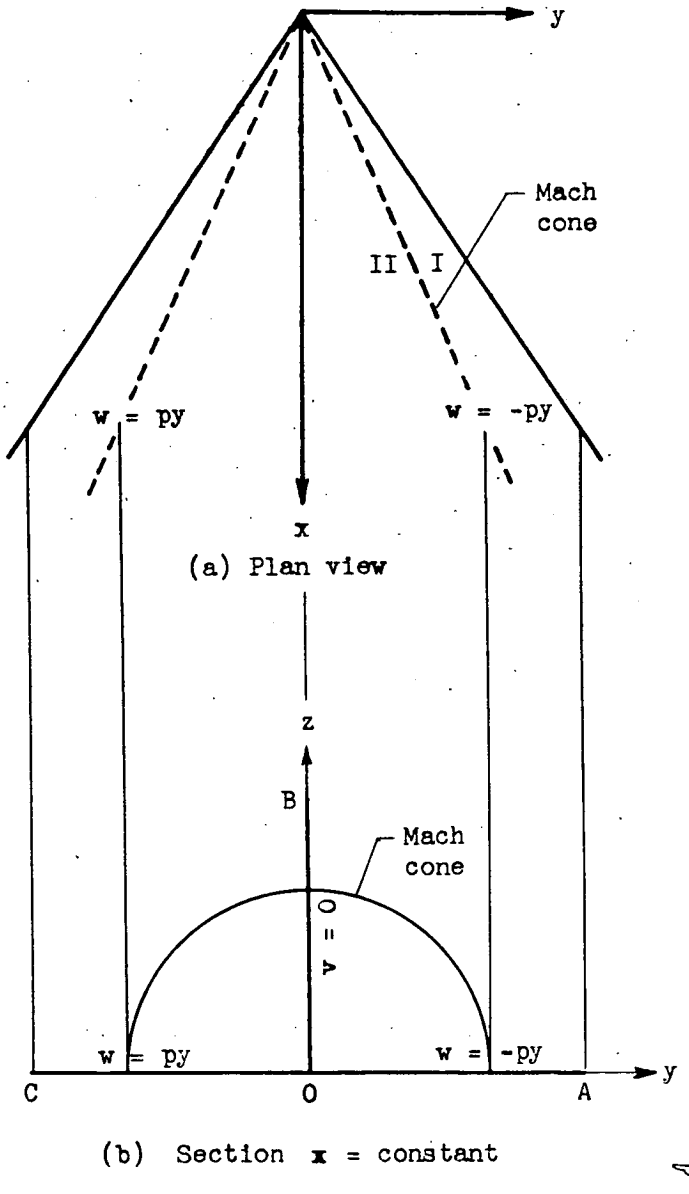

Figure 4. - Delta wing with linear symmetric twist obtained by reflection in x,z plane of figure for flow 3(b)..

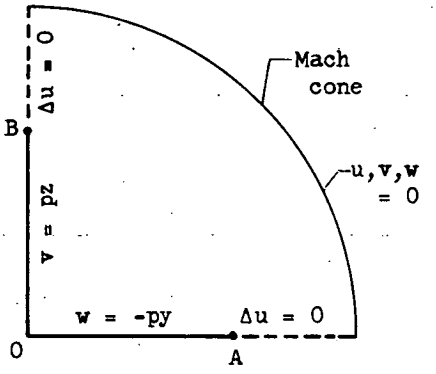

Figure 5. - Boundary conditions for quadrant of rolling cruciform delta with subsonic leading edges. Section x = constant.

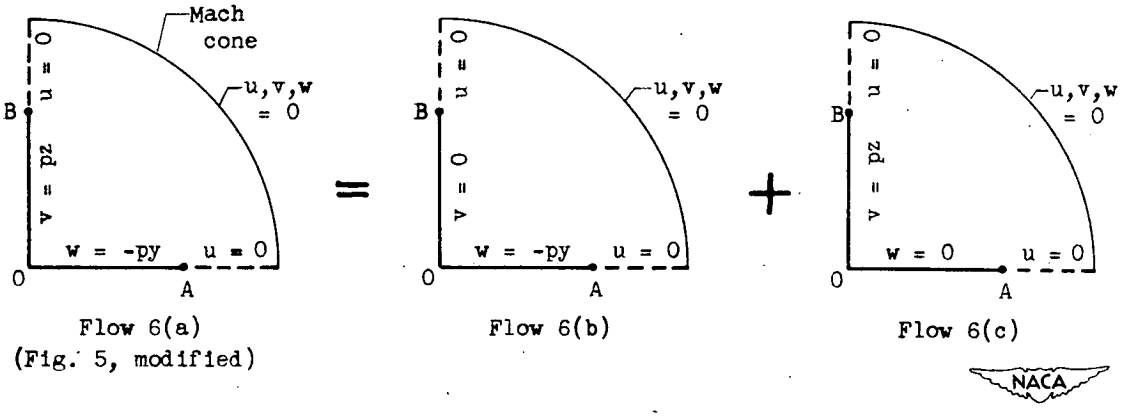

Flow 6(a)
(Fig. 5, modified)

Flow 6(b)

Flow 6(c)

Figure 6. - Superposition of simpler flows to obtain flow specified by modification of figure 5.

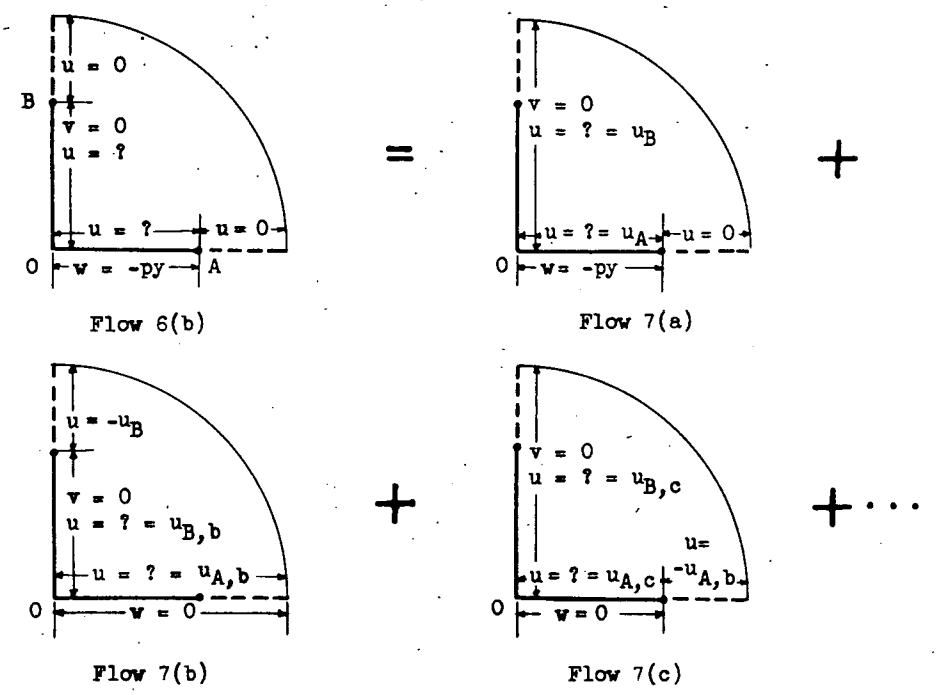

Figure 7. - Iteration scheme for determination of flow 6(b).

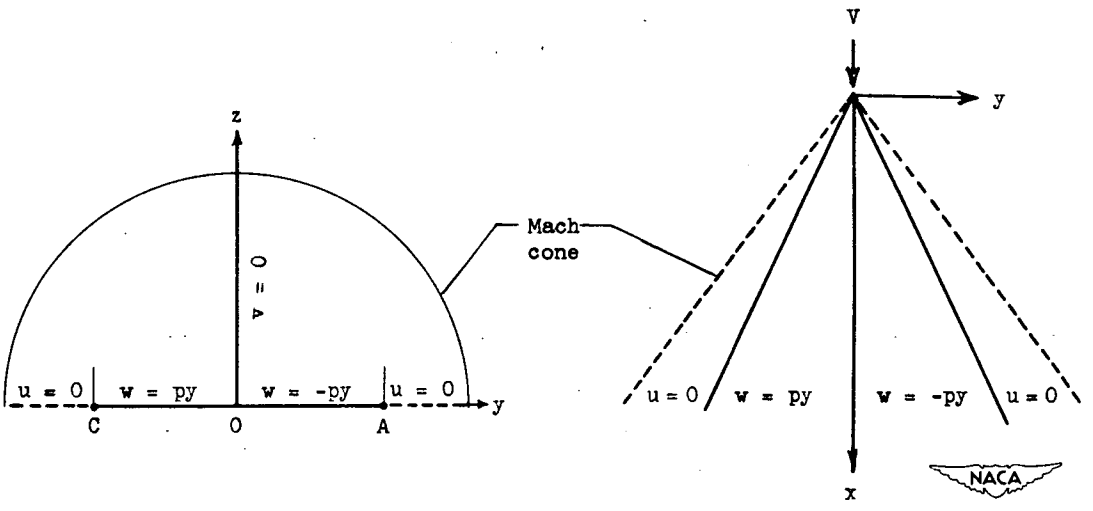

(a) Section x = constant (b) Plan view

Figure 8. - Delta wing with linear symmetric twist obtained by reflection in xz plane of figure for flow 7(a).

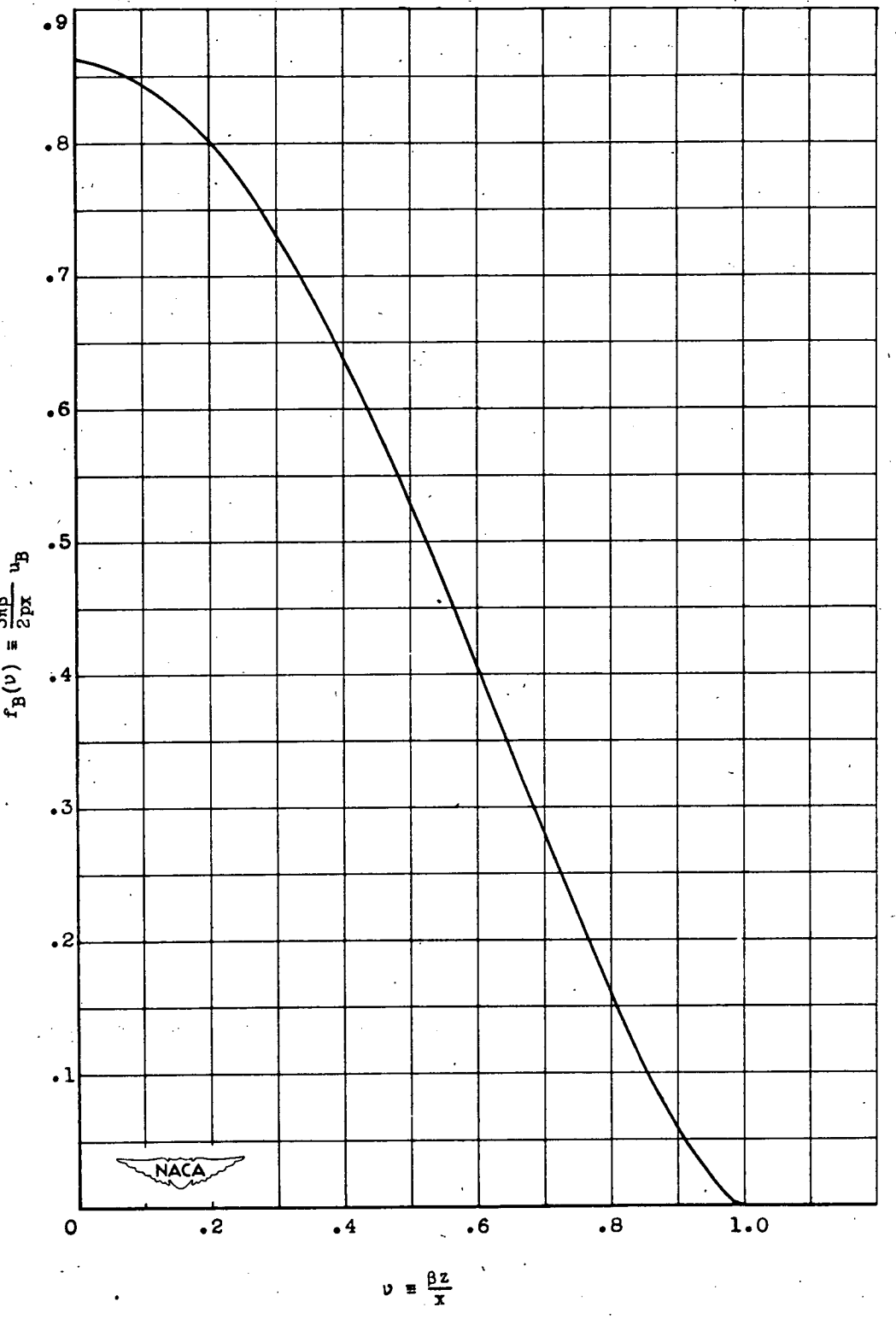

Figure 9. - Variation of $f_B(\nu) \equiv \frac{3\pi\beta^2}{2px} u_B(\nu)$ with ν for $m = 0.866$.

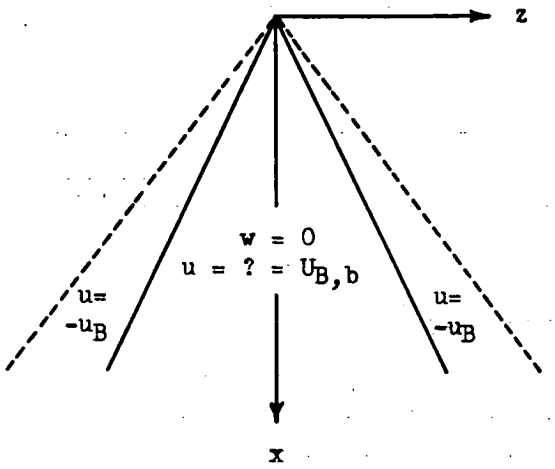

Figure 10. - Boundary conditions for solution for $u_{B,b}$ specified on lower surface of x,z plane. (Values of u specified for upper surface are of opposite sign.)

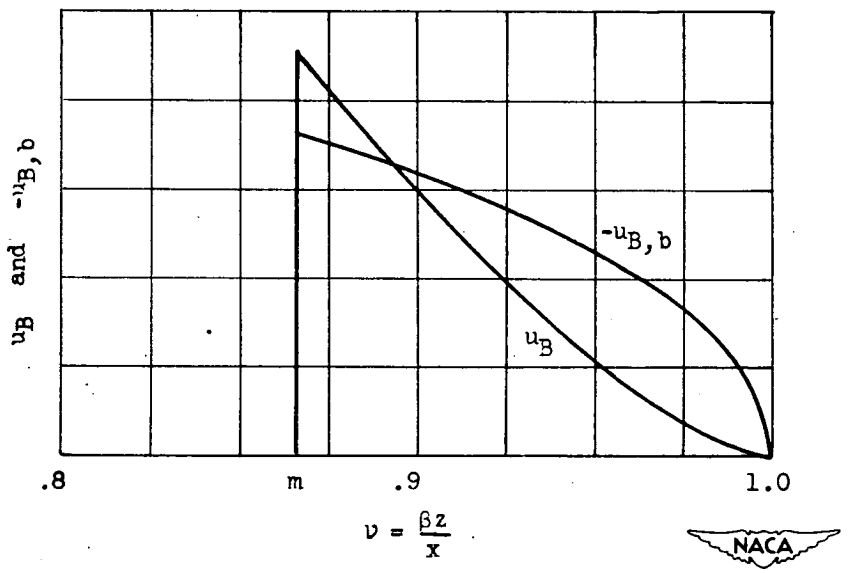

Figure 11. - Scheme for approximate cancellation of u_B by $u_{B,b}$ outboard of $\nu = m$. $m = 0.866$.

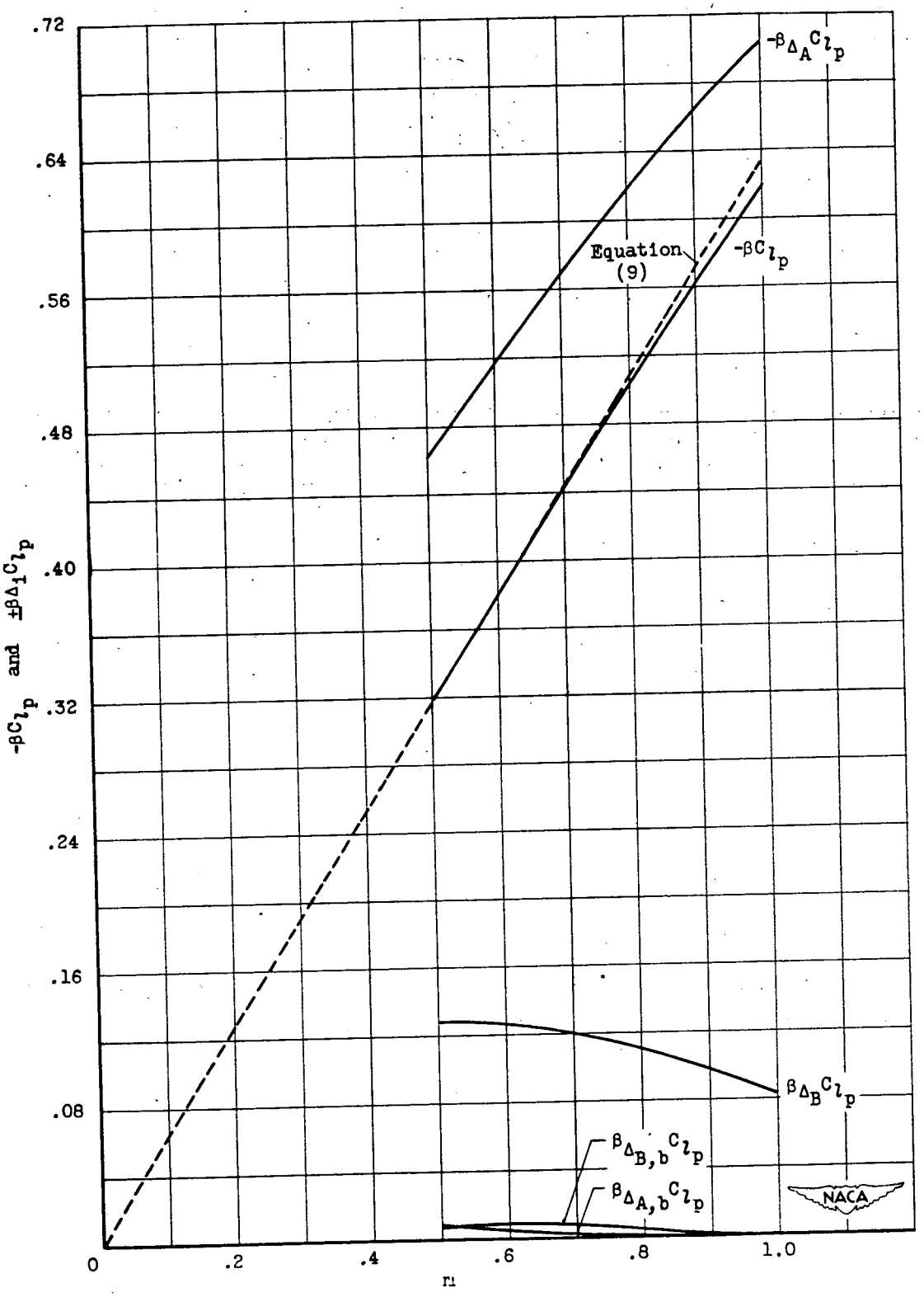

Figure 12. - Contributions of the first two iterations to $-\beta C_{l_p}$ for cruciform with subsonic leading edges.

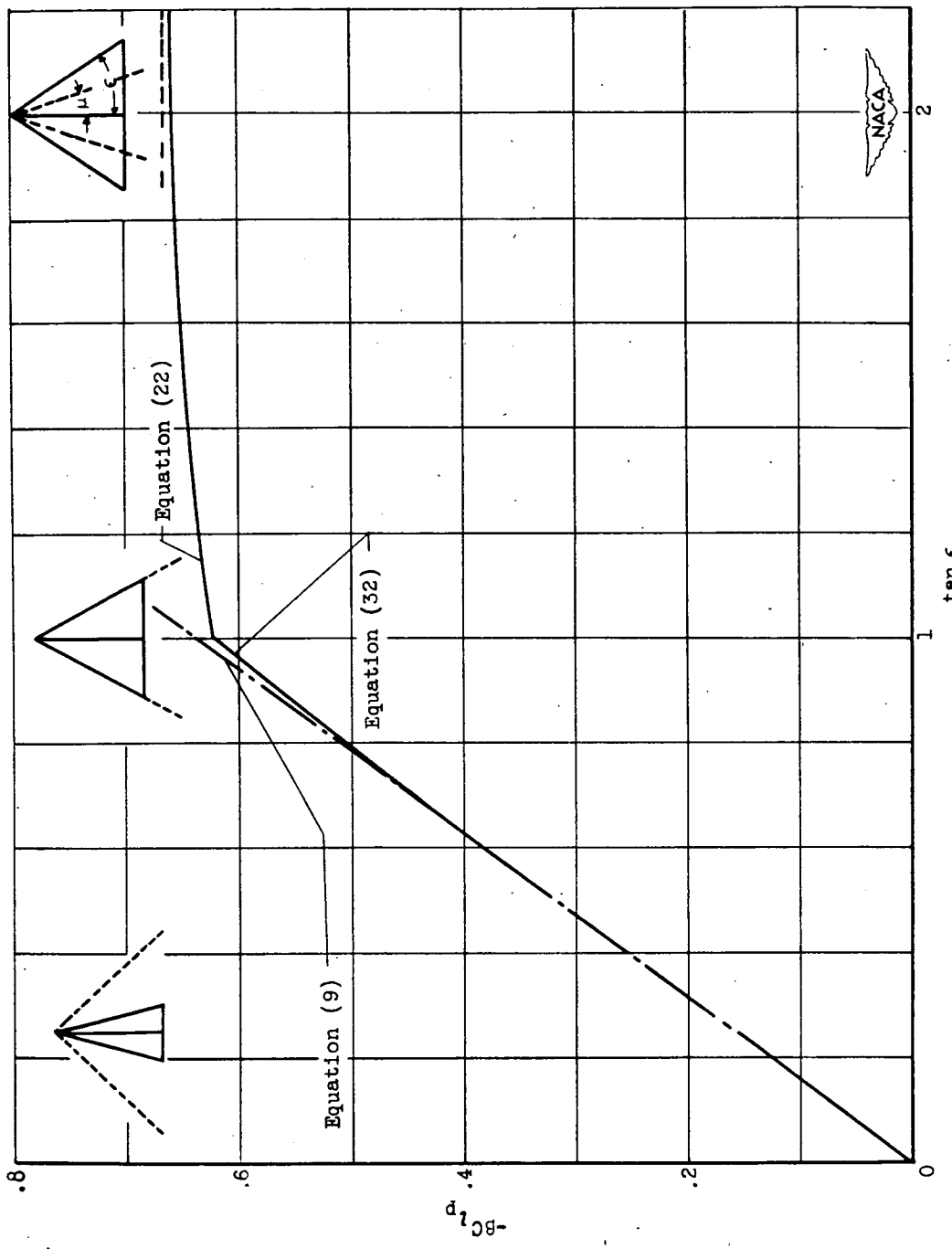

Figure 13. - Variation of damping-in-roll parameter with m for cruciform delta wing. Collected results.

Abstract

The damping in roll of cruciform delta wings in supersonic flow has been evaluated by means of small-disturbance (linearized) wing theory; both subsonic and supersonic component stream velocities normal to the leading edges have been considered. In addition, some known two-dimensional results for rotating multi-bladed laminae have been applied to obtain the loading when the number of panels is changed from four to an arbitrary number, under the restriction of low aspect ratio; the damping in roll has been determined explicitly for three panels. Finally, the damping for an infinite number of panels has been evaluated without restriction as to aspect ratio or Mach number.

Abstract

The damping in roll of cruciform delta wings in supersonic flow has been evaluated by means of small-disturbance (linearized) wing theory; both subsonic and supersonic component stream velocities normal to the leading edges have been considered. In addition, some known two-dimensional results for rotating multi-bladed laminae have been applied to obtain the loading when the number of panels is changed from four to an arbitrary number, under the restriction of low aspect ratio; the damping in roll has been determined explicitly for three panels. Finally, the damping for an infinite number of panels has been evaluated without restriction as to aspect ratio or Mach number.

Flow, Supersonic 1.1.2.3 S

NACA

Damping in Roll of Cruciform and Some Related Delta Wings at Supersonic Speeds.

By Herbert S. Ribner

NACA TN 2285

February 1951

(Abstract on Reverse Side)

Damping Derivatives - Stability 1.8.1.2.3 S

NACA

Damping in Roll of Cruciform and Some Related Delta Wings at Supersonic Speeds.

By Herbert S. Ribner

NACA TN 2285

February 1951

(Abstract on Reverse Side)